inorganics

MDPI

Article

Computational Characterization of Single-Electron Transfer Steps in Water Oxidation

Adiran de Aguirre [1,2], Ignacio Funes-Ardoiz [1,3] and Feliu Maseras [1,4,*]

1 Institute of Chemical Research of Catalonia (ICIQ), The Barcelona Institute of Science and Technology, Avgda. Països Catalans, 16, 43007 Tarragona, Catalonia, Spain; aaguirre@iciq.es (A.d.A.); ignacio.funes@rwth-aachen.de (I.F.-A.)
2 Departament de Química Física i Inorgànica, Universitat Rovira i Virgili, Marcel·lí Domingo s/n, 43007 Tarragona, Catalonia, Spain
3 Institute of Organic Chemistry, RWTH Aachen University, Landoltweg 1, 52074 Aachen, Germany
4 Departament de Química, Universitat Autònoma de Barcelona, 08193 Bellaterra, Catalonia, Spain
* Correspondence: fmaseras@iciq.es; Tel.: +34-977-920202

Received: 15 January 2019; Accepted: 22 February 2019; Published: 1 March 2019

Abstract: The presence of single-electron transfer (SET) steps in water oxidation processes catalyzed by first-row transition metal complexes has been recently recognized, but the computational characterization of this type of process is not trivial. We report a systematic theoretical study based on density functional theory (DFT) calculations on the reactivity of a specific copper complex active in water oxidation that reacts through two consecutive single-electron transfers. Both inner-sphere (through transition state location) and outer-sphere (through Marcus theory) mechanisms are analyzed. The first electron transfer is found to operate through outer-sphere, and the second one through inner-sphere. The current work proposes a scheme for the systematic study of single-electron transfer in water oxidation catalysis and beyond.

Keywords: Marcus theory; DFT; single-electron transfer; water oxidation; mechanisms

1. Introduction

One of the most promising reactions to replace the undesirable use of fossil fuels in energy production is the water splitting process triggered by sunlight, which generates oxygen and hydrogen from water. Molecular hydrogen generated in this way is generally known as solar-hydrogen or solar-fuel [1], and is used to store solar energy in chemical bonds, mimicking photosystem II in green plants and algae [2]. The chemical energy stored in the H–H bond can then be used as fuel, upon combustion with oxygen. The resulting water can then be used to reinitiate the overall process in a clean and green scheme. Alternatively, this hydrogen can be used to reduce CO_2 to produce more complex and convenient fuels [3].

From a chemical point of view, water splitting is a redox process formed by two half-reactions: water oxidation to molecular oxygen and protons, and the subsequent reduction of these protons to molecular hydrogen. Traditionally, the oxygen evolution reaction has always been the bottleneck, due to unfavorable thermodynamics and kinetics, and the design of efficient catalysts for this step is still a vast field of research [4–7]. Water oxidation, from a mechanistic point of view, involves the breaking of four H–O bonds, the release of 4 protons and 4 electrons, together with the formation of an O–O bond. This is associated with a high kinetic barrier, usually translated into the need of a very high overpotential [8].

One of the relevant strategies to overcome this high kinetic barrier is the development of molecular water oxidation catalysts (WOCs) based on transition metal complexes [9,10]. There are many synthetic and characterization techniques which allow for excellent control of the electronic and structural factors that are key in catalytic performance. The first steps in the development of water oxidation catalysts were those based on second- and third-row transition metals, such as Ru [11–18] or Ir [19–23]. More recently, molecular complexes based on first-row transition metals, such as Mn [24–27], Fe [28,29], Co [30,31], Ni [32], and Cu [33–37] have been reported, as they use more abundant and inexpensive elements.

Mechanistic and theoretical studies, mainly with Ru complexes, have been crucial to gain a deep understanding of the full mechanistic scenario involved in the water oxidation reaction [38]. In this context, two main pathways have been reported: water nucleophilic attack (WNA) and the interaction of two M–O species (I2M). Both mechanisms have been largely discussed by other groups [39,40], and any further details on them are outside the scope of this report. In 2015, we reported a step-by-step variant of the WNA mechanism, where the classical two-electron concerted reaction was divided in two sequential single-electron transfer (SET) steps that we called SET–WNA [41,42]. The mechanistic elucidation and, more specifically, the factors that control the oxidation of the ligand were key for further optimization of the catalyst, achieving a record overpotential value of 150 mV in basic pH [36].

Computational homogeneous catalysis has been mainly focused on two-electron transfers [43], but at present, the development of new photochemical and electrochemical reactions based on first-row transition metal catalysts has increased the popularity of SET steps [44,45]. From a theoretical perspective, these processes can proceed in two different ways: through an inner-sphere electron transfer step, where the electron "jumps" between two linked redox centers and can be described by classical transition state theory [46–48], or through an outer-sphere electron transfer step, where the two redox centers are not connected and the electron "hops" from one redox partner to the other. An example of an outer-sphere mechanism is the oxidation/reduction of a complex by means of a photoredox catalyst—a cornerstone of recent developments in photocatalysis [49].

A well-known approach to calculating these outer-sphere electron transfer processes is Marcus theory [50,51]. By applying this methodology, the activation barrier for an outer-sphere electron transfer between a donor and an acceptor species can be estimated. Although the theory appears in the 1950s, the direct application to transition metal catalyst calculations is not yet fully developed. Recently, the estimation of the barrier for outer-sphere single-electron transfer steps has been successfully applied, by our group [52,53] and others [54], to estimate energy barriers.

The number of reports on theoretical calculations of barriers for SET steps in homogeneous catalysis is increasing, but such studies are still scarce, particularly in the context of water oxidation. In this article, we revisit one of the systems we had previously studied, involving two SET steps, and reexamine each of them, in detail, to investigate their inner-sphere or outer-sphere nature. The water oxidation catalyst we studied is that presented in Figure 1, Cu-OPBAN (OPBAN = *o*-phenylenebis-(oxamidate). This system was found to follow the SET–WNA mechanism. We were able to characterize the existence of an intermediate and a transition state for an inner-sphere mechanism in the second transfer. For the first step, we postulated that the barrier was low, but we were not able to compute an accurate value. We will now present the computed barriers for outer-sphere mechanisms for each of the steps and compare them with the previous results.

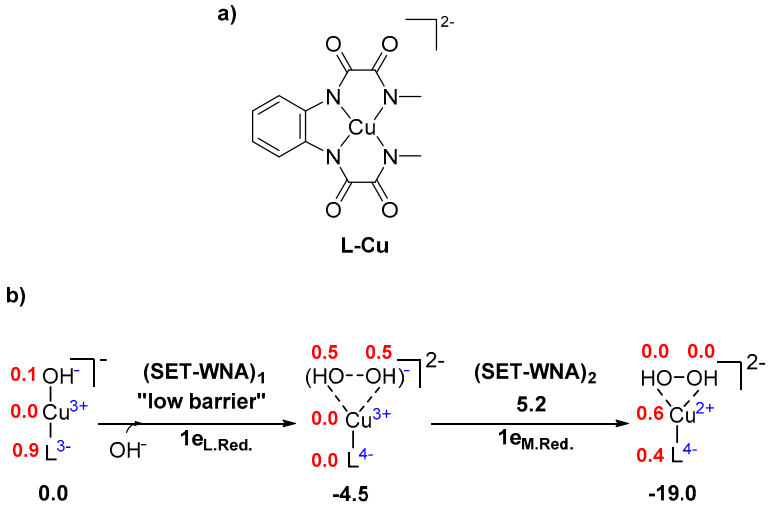

Figure 1. (**a**) The catalyst under study in this work. (**b**) single-electron transfer–water nucleophilic attack mechanism reported in [41]. Free energies (kcal/mol) in black, spin populations in red.

2. Results and Discussion

Inner-sphere electron transfer is characterized by a transition state, which yields an estimation of the barrier. The calculation may not be trivial, but it follows standard procedures well-known in the computational chemistry community. Outer-sphere electron transfer is not so simple, and we will apply Marcus theory to obtain the barriers. As the technique is less commonly used, we will briefly describe its main features. The initial idea of Marcus theory is that, for an outer-sphere electron transfer between two redox partners, there is a crossing point to go from the potential energy surface of the reactants to that of the products (Figure 2). However, in contrast to traditional transition state theory, this crossing point is associated not only with the structural changes of each species but also the solvation cage rearrangement surrounding each complex. The barrier is then estimated by considering the overlap between parabolic curves associated with the energies of both reactants and products. We apply, here, only the most simplified version of Marcus theory, without taking into account electronic coupling between the two states or electron tunneling.

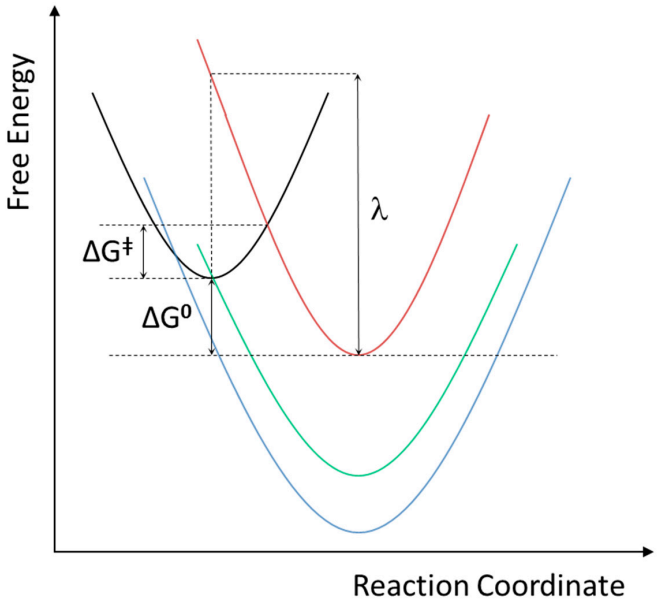

Figure 2. Schematic representation of the cases involved in Marcus theory. Red line = common reaction. Green line = barrierless reaction. Blue line = Marcus inversion region.

An interesting aspect of Marcus theory is the relation between the kinetic barrier of electron transfer and the reaction themodynamics. The most common case, which we will consider in this work, is that shown in red in Figure 2. The more exergonic the reaction, the lower the barrier for electron transfer. In the case where the intersection point between the curves for reactants and products is at the equilibrium coordinate of the reactant surface, no thermal activation is necessary, i.e., the reaction is barrierless (green line in Figure 2). When the intersection between both curves is at some point previous to the equilibrium coordinate of the reactants, the activation energy increases with the exothermicity of the process (blue line in Figure 2). The latter case has been labeled as "Marcus inversion region".

To estimate the energy barrier for the outer-sphere single-electron transfer $\Delta G^{\ddagger}$, we follow Equation (1). ΔG^0 is the standard free energy of the reaction step, i.e., the energy difference between reactants and products of the SET step, and λ is the reorganization energy of all nuclei and solvent molecules involved in the electron transfer step. The reorganization term λ is computed separately for each component: λ_N for the nuclear reorganization and λ_S for the solvent reorganization. The final value of λ is the sum of both components: λ_N and λ_S.

$$\Delta G^{\ddagger} = \frac{\left(\lambda + \Delta G^0\right)^2}{4\lambda} \quad (1)$$

The nuclear reorganization λ_N can be obtained by calculating the gas phase energy difference between the initial and final structure of each species participating in the SET. This is numerically shown in Equation (2), where D (donor) and A (acceptor) are the complexes participating in the SET step, the numbers 1 and 2 refer to initial and final structure, respectively, and α and β represent the electronic state of each complex. This term is related to the necessary energy for the system to distort the equilibrium structure to reach a proper structure for facilitation of electron transfer. The contribution of this component is expected to be smaller than λ_S, due to the small nuclei movement normally associated with outer-sphere electron transfer [50].

$$\lambda_N = D2\alpha + A2\beta - D1\alpha - A1\beta \quad (2)$$

The solvent reorganization λ_S is computed using the continuum solvent model. The value for λ_S is obtained from Equation (3). In this case, we keep the same geometry for both species (D1 and A1) and we compare the energy of the solvation cage between the initial and final electronic states ($[\delta]-[\varepsilon]$ and $[\alpha]-[\beta]$, respectively) of the SET step, for each species. In other words, it is the energy input needed to reorganize the solvent when the structural parameters of the redox partners change to facilitate the electron transfer. This methodology, when used to compute solvent reorganizations, has been shown to reproduce experimental results [55,56].

$$\lambda_S = D1[\delta] + A1[\varepsilon] - D1[\alpha] - A1[\beta] \quad (3)$$

Marcus theory is then applied to the following to estimate the outer-sphere barrier for the first electron transfer in our **CuL** system. Two models were considered. In the first model (Figure 3a), we considered that the electron transfer departs from the OH^- moiety (donor) and goes to the **1c** complex (acceptor). The associated free energy barrier for the outer-sphere electron transfer following this model, $\mathbf{MT_A\text{-}SET_1}$, is 23.0 kcal/mol from intermediate **1c** (Figure 3a). The product generated with this model would consist of a radical ·OH moiety and the one-electron reduced form of the complex, $\mathbf{MT_A\text{-}1d}$, in the singlet spin state. The energy of the resulting state of this first electron transfer is 8.3 kcal/mol. Then, the system could evolve through $\mathbf{MECP_A(S\text{-}T)}$ to result in the triplet spin state form of the catalyst, which is found at 3.2 kcal/mol below the singlet state.

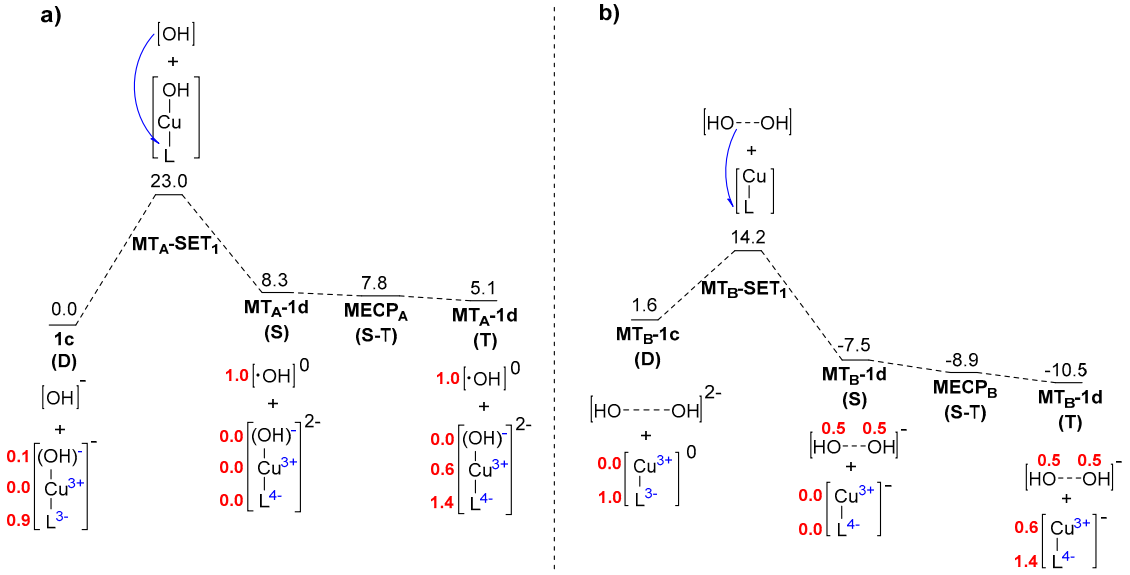

Figure 3. (**a**) Model A for the study of the outer-sphere SET from a OH^- moiety to **1c** complex applying Marcus theory. (**b**) Model B for the study of the outer-sphere SET from a cluster of two OH^- moieties to the neutral form of the catalyst, **MT_B-1c**. Free energies in kcal/mol. Red numbers correspond to the spin population.

The second model that we analyzed involves the electron transfer from a cluster of two OH^- moieties (donor) to the neutral form of the catalyst, **MT_B-1c** (acceptor) (Figure 3b). This cluster is generated from the initial reactants through release of the hydroxyl ligand from the complex, with a modest free energy cost of 1.6 kcal/mol. The calculated barrier for this model is 12.6 kcal/mol, **MT_B-SET_1** from previous intermediate **MT_B-1c**. Again, the product of the electron transfer step ends up in the singlet spin state form of the catalyst and evolves to the triplet spin state through **$MECP_B$(S-T)**. Finally, the product of this path, **MT_B-1d (T)**, is found at 12.1 kcal/mol below the reactants. The obtained values are in agreement with the expected dependence of the kinetic barrier on the thermodynamics of the reaction. As we can see from the comparison of our two models, model A, which is endergonic by 8.3 kcal/mol, has a higher kinetic barrier than model B which is exergonic by 9.1 kcal/mol. In both cases, the electron jumps from the OH moiety (model A) or from the HO···OH cluster (model B) to the ligand of the catalyst.

The calculated values for the two models are presented in Table 1. As expected, the nuclei reorganization term is much smaller than the solvent reorganization term.

Table 1. Marcus theory calculated values for the two models for the first SET step. Energies in kcal/mol.

Step	λ_S	λ_N	ΔG	$\Delta G^{\ddagger}$
MT_A-SET_1	74.4	0.1	8.3	23.0
MT_B-SET_1	61.9	5.4	−9.1	14.2

Interestingly, the barrier for model B is 14.2 kcal/mol, clearly affordable under the experimental reaction conditions. This indicates that this first electron transfer can proceed through an outer-sphere mechanism. The fact that we could not locate a transition state for this step, and that two different energies could be obtained for the same structures in the area where this transition state could be, suggests that the inner-sphere mechanism is not operative for this first electron transfer. Therefore, we conclude that the first SET step takes place through an outer-sphere mechanism with a barrier of 14.2 kcal/mol.

For the second electron transfer step, only model B was considered because the same number of atoms should be kept in both redox partners. The application of model B results in the final product,

while model A would form a double oxidized OH species that would not make chemical sense. The results from model B are depicted in Figure 4.

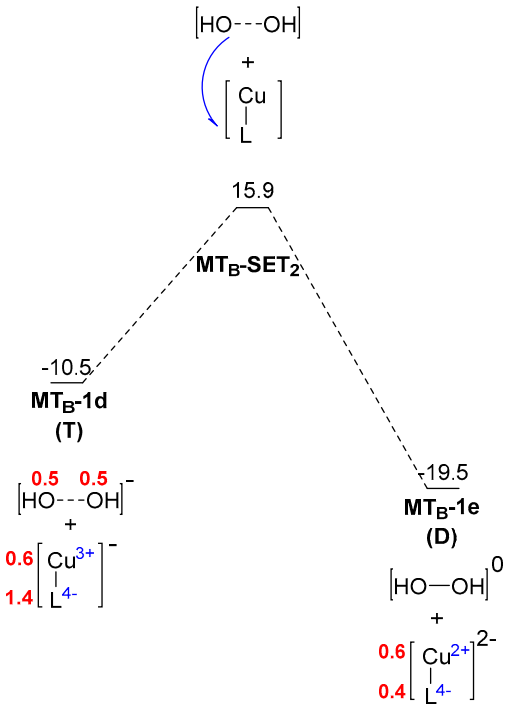

Figure 4. Free energy profile for the second SET applying Marcus theory. Energies in kcal/mol. Red numbers correspond to the spin population.

The activation barrier found with Marcus theory for the second single-electron transfer is at 26.4 kcal/mol, $\mathbf{MT_B\text{-}SET_2}$, from previous intermediate $\mathbf{MT_B\text{-}1d}$, which is considered as two fragments: the $[HO\cdots OH]^-$ cluster and the one electron reduced form of the initial catalyst. Remarkably, the free energy of **MTB-1e** (Figure 4), made of two separate fragments, is 0.5 kcal/mol below that of the adduct where the two fragments are together (Figure 1). There is a compensation between the entropic term favoring the separate fragments and the enthalpic term (weak chemical bonds) favoring the joint system.

The calculated values for the second electron transfer step are depicted in Table 2. In this case, we can see that the contribution of the nuclei rearrangement parameter is very high and almost equal to the solvent rearrangement. We attribute this discrepancy from the expected values (nuclei rearrangement should be much smaller than solvent rearrangement) to the energy difference between the [HO···OH] cluster before and after the SET step. In fact, if we divide the contribution coming from each redox partner, the contribution coming from the [HO···OH] cluster is 59.7 kcal/mol while for the Cu catalyst, it is only 1.2 kcal/mol. This is directly translated to a higher kinetic barrier and, thus, the reaction is not feasible through this mechanism.

Table 2. Marcus theory-calculated values for the second SET step. Energies in kcal/mol.

Step	λ_S	λ_N	ΔG	$\Delta G^{\ddagger}$
$\mathbf{MT_B\text{-}SET_2}$	62.1	60.9	−8.9	26.4

For the second electron transfer, the outer-sphere barrier of 26.4 kcal/mol is above what could be considered reasonable in the experimental conditions. It is, moreover, clearly higher than that for the inner-sphere barrier. Figure 1 reports a value of 9.7 kcal/mol, which should be corrected to 15.7 kcal/mol taking into account the existence of the more stable intermediate $\mathbf{MT_B\text{-}1d}$. We thus

conclude that for this second electron transfer the process takes place through an inner-sphere mechanism. The catalyst plays a significant role in the electron transfer internal coordinate and it is not a simple electron acceptor like in the outer-sphere mechanism.

We have thus shown that we can compute the barrier for both outer-sphere and inner-sphere single-electron transfer steps using, as a starting point, density functional theory (DFT) calculations. The accuracy is, in principle, similar to that of the already standard computational free energy profiles, which have been shown to be in reasonable agreement with the experiments and provide a roadmap to improved catalyst design. With the computational treatments we highlight, in this article, processes involving SET steps that can also be improved in a similar way.

3. Methods

All calculations were carried out by means of density functional theory as implemented in the Gaussian09 (Rev. D01) program package [57]. To make the current calculations easier to compare with the previous results on the system, the same description [36] was applied. This was the B3LYP-D3 functional [58,59], together with the basis set 6-31+G(d) for C, N, O, and H [60,61], and LANL2TZ(f) for Cu [62,63]. Water solvation was introduced implicitly using the SMD methodology [64]. All geometry optimizations were carried out in solution without symmetry restrictions. Free energy corrections were calculated at 298.15 K and 105 Pa pressure, including zero-point energy corrections (ZPE). Unless otherwise mentioned, all reported energy values are to be taken as free energies in solution. To compute the solvent reorganization term λ_S, we used the keywords *NonEq = write* and *NonEq = read* in Gaussian09 to store and read the solvent cage.

A dataset collection of computational results is available in the ioChem-BD repository [65] and can be accessed via https://doi.org/10.19061/iochem-bd-1-112. Cartesian coordinates for all stationary points are provided also as Supplementary Materials.

4. Conclusions

Single-electron transfer processes in water oxidation can take place through either inner-sphere or outer-sphere mechanisms, and their barriers can be computed by computational chemistry based on DFT methods. The barrier for inner-sphere mechanisms can be measured from the free energy of the associated transition states, while the barrier for outer-sphere mechanisms can be computed through application of Marcus theory. In the specific copper catalyst studied for water oxidation, two transfers are involved, where the first takes place through the outer-sphere, and the second through the inner-sphere. We recommend that both mechanisms should be tried for any single-electron transfer process. The inner-sphere electron transfer requires the characterization of a transition state. If this does not exist, we suggest that the process should operate through the outer-sphere mechanism, which can be evaluated through the application of Marcus theory. When the transition state can be located, the barriers to both inner- and outer-sphere can be computed, and must be compared. Additionally, efficient characterization of single-electron transfer processes can provide abundant information on steps that are difficult to characterize experimentally and facilitate the optimization of water oxidation processes.

Supplementary Materials: The following are available online at http://www.mdpi.com/2304-6740/7/3/32/s1, Cartesian coordinates of all stationary points in the manuscript.

Author Contributions: Conceptualization, F.M. and I.F.-A.; investigation, A.d.A.; writing—original draft preparation, A.d.A. and I.F.-A; writing—review and editing, A.d.A., I.F.-A. and F.M.; funding acquisition, F.M.

Funding: This research was funded by the CERCA Programme (Generalitat de Catalunya), and MINECO (grant CTQ2017-87792-R to F.M., BES-2015-073012 to A.d.A. and SVP-2014-068662 to I.F.-A.)

Conflicts of Interest: The authors declare no conflict of interest.

References

1. Nowotny, J.; Sorrell, C.C.; Sheppard, L.R.; Bak, T. Solary-hydrogen: Environmentally safe fuel for the future. *Int. J. Hydrogen Energy* **2005**, *30*, 521–544. [CrossRef]
2. Cox, N.; Pantazis, D.A.; Neese, F.; Lubitz, W. Biological water oxidation. *Acc. Chem. Res.* **2013**, *46*, 1588–1596. [CrossRef] [PubMed]
3. Bergthorson, J.M. Recyclable metal fuels for clean and compact zero-carbon power. *Prog. Energy Combust. Sci.* **2018**, *68*, 169–196. [CrossRef]
4. Sun, L.; Hammarstrom, L.; Akermark, B.; Styring, S. Towards artificial photosynthesis: Ruthenium–manganese chemistry for energy production. *Chem. Soc. Rev.* **2001**, *30*, 36–49. [CrossRef]
5. Alstrum-Acevedo, J.H.; Brennaman, M.K.; Meyer, T.J. Chemical approeaches to artifical photosynthesis. 2. *Inorg. Chem.* **2005**, *44*, 6802–6827. [CrossRef] [PubMed]
6. Nocera, D.G. The artifical leaf. *Acc. Chem. Res.* **2012**, *45*, 767–776. [CrossRef] [PubMed]
7. Youngblood, W.J.; Lee, S.-H.A.; Kobayashi, Y.; Hernandez-Pagan, E.A.; Hoertz, P.G.; Moore, T.A.; Moore, A.L.; Gust, D.; Mallouk, T.E. Photoassisted overall water splitting in a visible light-absorbing dye-sensitized photoelectrochemical cell. *J. Am. Chem. Soc.* **2009**, *131*, 926–927. [CrossRef] [PubMed]
8. Mckone, J.R.; Lewis, N.S.; Gray, H.B. Will solar-driven water-splitting devices see the light of day? *Chem. Mater.* **2014**, *26*, 407–414. [CrossRef]
9. Garrido-Barros, P.; Gimbert-Suriñach, C.; Matheu, R.; Sala, X.; Llobet, A. How to make an efficient and robust molecular catalyst for water oxidation. *Chem. Soc. Rev.* **2017**, *46*, 6088–6098. [CrossRef] [PubMed]
10. Kärkaäs, M.D.; Verho, O.; Johnston, E.V.; Åkermark, B. Artificial photosynthesis: Molecular systems for catalytic water oxidation. *Chem. Rev.* **2014**, *114*, 11863–12001. [CrossRef] [PubMed]
11. Sala, X.; Romero, I.; Rodríguez, M.; Escriche, L.; Llobet, A. Molecular catalysts that oxidize water to dioxygen. *Angew. Chem. Int. Ed.* **2009**, *48*, 2842–2852. [CrossRef] [PubMed]
12. Romain, S.; Vigara, L.; Llobet, A. Oxygen–Oxygen bond formation pathways promoted by ruthenium complexes. *Acc. Chem. Res.* **2009**, *42*, 1944–1953. [CrossRef] [PubMed]
13. Duan, L.; Bozoglian, F.; Mandal, S.; Stewart, B.; Privalov, T.; Llobet, A.; Sun, L. A molecular ruthenium catalyst with water-oxidation activity comparable to that of photosystem II. *Nat. Chem.* **2012**, *4*, 418–423. [CrossRef] [PubMed]
14. Neudeck, S.; Maji, S.; Lopez, I.; Meyer, S.; Meyer, F.; Llobet, A. New powerful and oxidatively rugged dinuclear Ru water oxidation catalyst: Control of mechanistic pathways by tailored ligand design. *J. Am. Chem. Soc.* **2014**, *136*, 24–27. [CrossRef] [PubMed]
15. Vigara, L.; Ertem, M.Z.; Planas, N.; Bozoglian, F.; Leidel, N.; Dau, H.; Haumann, M.; Gagliardi, L.; Cramer, C.J.; Llobet, A. Experimental and quantum chemical characterization of the water oxidation cycle cataysed by $[Ru^{II}(damp)(bpy)(H_2O)]^{2+}$. *Chem. Sci.* **2012**, *3*, 2576–2586. [CrossRef]
16. Concepcion, J.J.; Jurss, J.W.; Brennaman, M.K.; Hoertz, P.G.; Patrocinio, A.O.T.; Murakami Iha, N.Y.; Templeton, J.L.; Meyer, T.J. Making oxygen with ruthenium complexes. *Acc. Chem. Res.* **2009**, *42*, 1954–1965. [CrossRef] [PubMed]
17. Zong, R.; Thummel, R.P. A new family of Ru complexes for water oxidation. *J. Am. Chem. Soc.* **2005**, *127*, 12802–12803. [CrossRef] [PubMed]
18. Schulze, M.; Kunz, V.; Frischmann, P.D.; Würthner, F. A supramolecular ruthenium macrocycle with high catalytic activity for water oxidation that mechanistically mimics photosystem II. *Nat. Chem.* **2016**, *8*, 576–583. [CrossRef] [PubMed]
19. Hull, J.F.; Balcells, D.; Blakemore, J.D.; Incarvito, C.D.; Eisenstein, O.; Brudvig, G.W.; Crabtree, R.H. Highly active and robust Cp* iridium complexes for catalytic water oxidation. *J. Am. Chem. Soc.* **2009**, *131*, 8730–8731. [CrossRef] [PubMed]
20. Lalrempuia, R.; McDaniel, N.D.; Müller-Bunz, H.; Bernhard, S.; Albrecht, M. Water oxidation catalyzed by strong carbene-type donor-ligand complexes of iridium. *Angew. Chem. Int. Ed.* **2010**, *49*, 9765–9768. [CrossRef] [PubMed]
21. Thomsen, J.M.; Sheehan, S.W.; Hashmi, S.M.; Campos, J.; Hintermair, U.; Crabtree, R.H.; Brudvig, G.W. Electrochemical activation of Cp* iridium complexes for electrode-driven water-oxidation catalysis. *J. Am. Chem. Soc.* **2014**, *136*, 13826–13834. [CrossRef] [PubMed]

22. Woods, J.A.; Bernhard, S.; Albrecht, M. Recent advances in the field of iridium-catalyzed molecular water oxidation. In *Molecular Water Oxidation Catalysis*; Llobet, A., Ed.; John Wiley & Sons, Ltd.: New York, NY, USA, 2014; pp. 113–134.
23. McDaniel, N.D.; Coughlin, F.J.; Tinker, L.L.; Bernhard, S. Cyclometalated iridium(III) aquo complexes: Efficient and tunable catalysts for the homogeneous oxidation of water. *J. Am. Chem. Soc.* **2008**, *130*, 210–217. [CrossRef] [PubMed]
24. Limburg, J.; Vrettos, J.S.; Liable-Sands, L.M.; Rheingold, A.L.; Crabtree, R.H.; Brudvig, G.W. A functional model for O–O bond formation by the O_2-evolving complex in photosystem II. *Science* **1999**, *283*, 1524–1527. [CrossRef] [PubMed]
25. Shimazaki, Y.; Nagano, T.; Takesue, H.; Ye, B.-H.; Tani, F.; Naruta, Y. Characterization of a dinuclear MnV=O complex and is efficient evolution of O_2 in the presence of water. *Angew. Chem. Int. Ed.* **2004**, *43*, 98–100. [CrossRef] [PubMed]
26. Limburg, J.; Brudvig, G.W.; Crabtree, R.H. O_2 evolution and permanganate formation from high-valent manganese complexes. *J. Am. Chem. Soc.* **1997**, *119*, 2761–2762. [CrossRef]
27. Pushkar, Y.; Davis, K.M.; Palenik, M.C. Model of the oxygen evolving complex which is highly predisposed to O–O bond formation. *J. Phys. Chem. Lett.* **2018**, *9*, 3525–3531. [CrossRef] [PubMed]
28. Ellis, W.C.; McDaniel, N.D.; Bernhard, S.; Collins, T.J. Fast water oxidation using iron. *J. Am. Chem. Soc.* **2010**, *132*, 10990–10991. [CrossRef] [PubMed]
29. Wickramasinghe, L.D.; Zhou, R.; Zong, R.; Vo, P.; Gagnon, K.J.; Thummel, R.P. Iron complexes of square planar tetradentate polypyridyl-type ligands as catalysts for water oxidation. *J. Am. Chem. Soc.* **2015**, *137*, 13260–13263. [CrossRef] [PubMed]
30. Wasylenko, D.J.; Ganesamoorthy, C.; Borau-Garcia, J.; Berlinguette, C.P. Electrochemical evidence for catalytic water oxidation mediated by a high-valent cobalt complex. *Chem. Commun.* **2011**, *47*, 4249–4251. [CrossRef] [PubMed]
31. Rigsby, M.L.; Mandal, S.; Nam, W.; Spencer, L.C.; Llobet, A.; Stahl, S.S. Cobalt analogs of Ru-based water oxidation catalysts: Overcoming thermodynamic instability and kinetic lability to achieve electrocatalytic O_2 evolution. *Chem. Sci.* **2012**, *3*, 3058–3062. [CrossRef]
32. Han, Y.; Wu, Y.; Lai, W.; Cao, R. Electrocatalytic water oxidation by a water-soluble nickel porphyrin complex at netural pH with low overpotential. *Inorg. Chem.* **2015**, *54*, 5604–5613. [CrossRef] [PubMed]
33. Barnett, S.M.; Goldberg, K.I.; Mayer, J.M. A soluble copper-bipyridine water-oxidation electrocatalyst. *Nat. Chem.* **2012**, *4*, 498–502. [CrossRef] [PubMed]
34. Zhang, M.-T.; Chen, Z.; Kang, P.; Meyer, T.J. Electrocatalytic water oxidation with a copper(II) polypeptide complex. *J. Am. Chem. Soc.* **2013**, *135*, 2048–2051. [CrossRef] [PubMed]
35. Zhang, T.; Wang, C.; Liu, S.; Wang, J.-L.; Lin, W. A biomimetic copper water oxidation catalyst with low overpotential. *J. Am. Chem. Soc.* **2014**, *136*, 273–281. [CrossRef] [PubMed]
36. Garrido-Barros, P.; Funes-Ardoiz, I.; Drouet, S.; Benet-Buchholz, J.; Maseras, F.; Llobet, A. Redox non-innocent ligand controls water oxidation overpotential in a new family of mononuclear Cu-based efficient catalysts. *J. Am. Chem. Soc.* **2015**, *137*, 6758–6761. [CrossRef] [PubMed]
37. Fisher, K.J.; Materna, K.L.; Mercado, B.Q.; Crabtree, R.H.; Brudvig, G.W. Electrocatalytic water oxidation by a copper(II) complex of an oxidation-resistant ligand. *ACS Catal.* **2017**, *7*, 3384–3387. [CrossRef]
38. Liao, R.-Z.; Siegbahn, P.E.M. Quantum chemical modeling of homogeneous water oxidation catalysis. *ChemSusChem* **2017**, *10*, 4236–4263. [CrossRef] [PubMed]
39. Sala, X.; Maji, S.; Bofill, R.; García-Anton, J.; Escriche, L.; Llobet, A. Molecular water oxidation mechanisms followed by transition metals: State of the art. *Acc. Chem. Res.* **2014**, *47*, 504–516. [CrossRef] [PubMed]
40. Concepcion, J.J.; Tsai, M.-K.; Muckerman, J.T.; Meyer, T.J. Mechanism of water oxidation by single-site ruthenium complex catalysts. *J. Am. Chem. Soc.* **2010**, *132*, 1545–1557. [CrossRef] [PubMed]
41. Funes-Ardoiz, I.; Garrido-Barros, P.; Llobet, A.; Maseras, F. Single electron transfer steps in water oxidation catalysis. Redefining the mechanistic scenario. *ACS Catal.* **2017**, *7*, 1712–1719. [CrossRef]
42. de Aguirre, A.; Garrido-Barros, P.; Funes-Ardoiz, I.; Maseras, F. The role of electron-donor substituents in the family of OPBAN-Cu water oxidation catalysts: Effect on the degradation pathways and efficiency. *Eur. J. Inorg. Chem.* **2019**. [CrossRef]

43. Sameera, W.M.C.; Maseras, F. Transition metal catalysis by density functional theory and density functional theory/molecular mechanics. *WIREs Comput. Mol. Sci.* **2012**, *2*, 375–385. [CrossRef]
44. Shaik, S.; Kumar, D.; de Visser, S.P.; Altun, A.; Thiel, W. Theoretical perspective on the structure and mechanism of cytochrome P450 enzymes. *Chem. Rev.* **2005**, *105*, 2279–2328. [CrossRef] [PubMed]
45. Ye, S.; Geng, C.-Y.; Shaik, S.; Neese, F. Electronic structure analysis of multistate reactivity in transition metal catalyzed reactions: The case of C–H bond activation by non-heme iron(IV)–oxo cores. *Phys. Chem. Chem. Phys.* **2013**, *15*, 8017–8030. [CrossRef] [PubMed]
46. Funes-Ardoiz, I.; Nelson, D.J.; Maseras, F. Halide abstraction competes with oxidative addition in the reactions of aryl halides with [Ni($PMe_nPh_{(3-n)}$)$_4$]. *Chem. Eur. J.* **2017**, *23*, 16728–16733. [CrossRef] [PubMed]
47. Nelson, D.J.; Maseras, F. Steric effects determine the mechanisms of reaction between bis(*N*-heterocyclic carbene)–nickel(0) complexes and aryl halides. *Chem. Commun.* **2018**, *54*, 10646–10649. [CrossRef] [PubMed]
48. Truhlar, D.G.; Garrett, B.C.; Klippenstein, S.J. Current Status of transition-state theory. *J. Phys. Chem.* **1996**, *100*, 12771–12800. [CrossRef]
49. Prier, C.K.; Rankic, D.A.; MacMillan, D.W.C. Visible light photoredox catalysis with transition metal complexes: Applications in organic synthesis. *Chem. Rev.* **2013**, *113*, 5322–5363. [CrossRef] [PubMed]
50. Marcus, R.A. On the theory of oxidation-reduction reactions involving electron transfer. *J. Chem. Phys.* **1956**, *24*, 966–978. [CrossRef]
51. Marcus, R.A. Electron transfer reactions in chemistry: Theory and experimental (Nobel lecture). *Angew. Chem. Int. Ed. Engl.* **1993**, *32*, 1111–1121. [CrossRef]
52. Fernandez-Alvarez, V.M.; Maseras, F. Computational characterization of the mechanism for the light-driven catalytic trichloromethylation of acylpyridines. *Org. Biomol. Chem.* **2017**, *15*, 8641–8647. [CrossRef] [PubMed]
53. de Aguirre, A.; Funes-Ardoiz, I.; Maseras, F. Four oxidation states in a single photoredox Ni-based catalytic cycle: A computational study. *Angew. Chem. Int. Ed.* **2019**. [CrossRef]
54. Qi, Z.-H.; Ma, J. Dual role of a photocatalyst: Generation of Ni(0) catalyst and promotion of catalytic C–N bond formation. *ACS Catal.* **2018**, *8*, 1456–1463. [CrossRef]
55. Moia, D.; Vaissier, V.; Lopez-Duarte, I.; Torres, T.; Nazeeruddin, M.K.; O'Regan, B.C.; Nelson, J.; Barnes, P.R.F. The reorganization energy of intermolecular hole hopping between dyes anchored to surfaces. *Chem. Sci.* **2014**, *5*, 281–290. [CrossRef]
56. Vaissier, V.; Barnes, P.; Kirkpatrick, J.; Nelson, J. Influence of polar medium on the reorganization energy of charge transfer between dyes in a dye sensitized film. *Phys. Chem. Chem. Phys.* **2013**, *15*, 4804–4814. [CrossRef] [PubMed]
57. Frisch, M.J.; Trucks, G.W.; Schlegel, H.B.; Scuseria, G.E.; Robb, M.A.; Cheeseman, J.R.; Scalmani, G.; Barone, V.; Mennucci, B.; Petersson, G.A.; et al. *Gaussian 09, Revision D.01*; Gaussian, Inc.: Wallingford, CT, USA, 2009.
58. Becke, A.D. A new mixing of Hartree-Fock and local density-functional theories. *J. Chem. Phys.* **1993**, *98*, 5648–5652. [CrossRef]
59. Grimme, S.; Antony, J.; Ehrlich, S.; Krieg, H. A consistent and accurate ab initio parmetrization of density functional dispersion correction (DFT-D) for the 94 elements H–Pu. *J. Chem. Phys.* **2010**, *132*, 154104. [CrossRef] [PubMed]
60. Francl, M.M.; Petro, W.J.; Hehre, W.J.; Binkley, J.S.; Gordon, M.S.; DeFrees, D.J.; Pople, J.A. Self-consistent molecular orbital methods. XXIII. A polarization-type basis set for second-row elements. *J. Chem. Phys.* **1982**, *77*, 3654–3665. [CrossRef]
61. Clark, T.; Chandrasekhar, J.; Schleyer, P.V.R. Efficient diffuse function-augmented basis sets for anion. III. The 3-21+G basis set for first-row elements, Li–F. *J. Comput. Chem.* **1983**, *4*, 294–301. [CrossRef]
62. Ehlers, A.W.; Böhme, M.; Dapprich, S.; Gobbi, A.; Höllwarth, A.; Jonas, V.; Köhler, K.F.; Stegmann, R.; Veldkamp, A.; Frenking, G. A set of f-polarization functions for pseudo-potential basis sets of the transition metals Sc–Cu, Y–Ag and La–Au. *Chem. Phys. Lett.* **1993**, *208*, 111–114. [CrossRef]
63. Roy, L.E.; Hay, P.J.; Martin, R.L. Revised basis sets for the LANL effective core potentials. *J. Chem. Theory Comput.* **2008**, *4*, 1029–1031. [CrossRef] [PubMed]

64. Marenich, A.V.; Cramer, C.J.; Truhlar, D.G. Universal solvation model based on solute electron density and on a continuum model of the solvent defined by the bulk dielectric constant and atomic surface tensions. *J. Phys. Chem. B* **2009**, *113*, 6378–6396. [CrossRef] [PubMed]
65. Alvarez-Moreno, M.; de Graaf, C.; Lopez, N.; Maseras, F.; Poblet, J.M.; Bo, C. Managing the computational chemistry big data problem: The ioChem-BD platform. *J. Chem. Inf. Model.* **2015**, *55*, 95–103. [CrossRef] [PubMed]